Magnetic Reconnection at a Thin Current Sheet Separating Two Interlaced Flux Tubes at the Earth's Magnetopause

I. Kacem, C. Jacquey, V. Génot, B. Lavraud, Y. Vernisse, A. Marchaudon, Olivier Le Contel, Hugo Breuillard, T. D. Phan, H. Hasegawa, et al.

Magnetic reconnection at a thin current sheet separating two interlaced flux tubes at the Earth's magnetopause

I. Kacem[1], C. Jacquey[1], V. Génot[1], B. Lavraud[1], Y. Vernisse[1], A. Marchaudon[1], O. Le Contel[2], H. Breuillard[2], T. D. Phan[3], H. Hasegawa[4], M. Oka[3], K. J. Trattner[5], C. J. Farrugia[6], K. Paulson[6], J. P. Eastwood[7], S. A. Fuselier[8,9], D. Turner[10], S. Eriksson[5], F. Wilder[5], C. T. Russell[11], M. Øieroset[3], J. Burch[8], D. B. Graham[12], J.-A. Sauvaud[1], L. Avanov[13], M. Chandler[14], V. Coffey[14], J. Dorelli[13], D. J. Gershman[13], B. L. Giles[13], T. E. Moore[13], Y. Saito [4], L.-J. Chen[13], and E. Penou[1]

[1] Institut de Recherche en Astrophysique et Planétologie, CNRS, UPS, CNES, Université de Toulouse, France.

[2] Laboratoire de Physique des Plasmas, Palaiseau, France.

[3] Space Sciences Laboratory, Berkeley, CA.

[4] Institute of Space and Astronautical Science, JAXA, Sagamihara, Japan.

[5] Laboratory for Atmospheric and Space Physics, University of Colorado Boulder, Colorado, USA.

[6] University of New Hampshire, Durham, NH.

[7] The Blackett Laboratory, Imperial College, London, UK.

[8] Southwest Research Institute, San Antonio, TX.

[9] University of Texas at San Antonio, San Antonio, TX.

[10] Space Sciences Department, The Aerospace Corporation, El Segundo, California, USA.

[11] UCLA, Institute of Geophysics, Earth Planetary and Space Sciences, Los Angeles, United States.

[12] Swedish Institute of Space Physics, Uppsala, Sweden.

[13] NASA Goddard Space Flight Center, Greenbelt, MD.

[14] NASA Marshall Space Flight Center, Huntsville, AL.

Issaad Kacem (issaad.kacem@irap.omp.eu)

Key Points:

- Characterization of the scale, geometry and propagation of an ion scale current structure resulting from the interaction between interlaced flux tubes.
- Some signatures of magnetic reconnection are found at the interaction interface
- The intrinsic properties of this event are inconsistent with a single, homogenous helicoidal magnetic structure as expected from a typical Flux Transfer Event (FTE).

Abstract

The occurrence of spatially and temporally variable reconnection at the Earth's magnetopause leads to the complex interaction of magnetic fields from the magnetosphere and magnetosheath. Flux Transfer Events (FTEs) constitute one such type of interaction. Their main characteristics are 1/ an enhanced core magnetic field magnitude and 2/ a bipolar magnetic field signature in the component normal to the magnetopause, reminiscent of a large-scale helicoidal flux tube magnetic configuration. However, other geometrical configurations which do not fit this classical picture have also been observed. Using high-resolution measurements from the Magnetospheric Multiscale mission (MMS), we investigate an event in the vicinity of the Earth's magnetopause on November 7, 2015. Despite signatures that, at first glance, appear consistent with a classic FTE, based on detailed geometrical and dynamical analyses as well as on topological signatures revealed by suprathermal electron properties, we demonstrate that this event is not consistent with a single, homogenous helicoidal structure. Our analysis rather suggests that it consists of the interaction of two separate sets of magnetic field lines with different connectivities. This complex three-dimensional interaction constructively conspires to produce signatures partially consistent with that of an FTE. We also show that, at the interface between the two sets of field lines, where the observed magnetic pile up occurs, a thin and strong current sheet forms with a large ion jet, which may be consistent with magnetic flux dissipation through magnetic reconnection in the interaction region.

1 Introduction

Magnetic reconnection is a ubiquitous and fundamental process in space plasma physics. When the Interplanetary Magnetic Field (IMF) is directed southward, magnetic reconnection occurs at the Earth's dayside magnetopause current sheet and in the magnetotail current sheet as a result of the interaction between the solar wind and the Earth's magnetic field lines. Magnetic reconnection plays a major role in magnetospheric dynamics [*Dungey,* 1961]. It governs the transport of energy, momentum and plasma from the solar wind into the Earth's magnetosphere [*Dungey,* 1961; *Lemaire and Roth,* 1978; *Biernat* et al., 1991; *Eastwood et al.,* 2013]. Indeed, magnetic reconnection is associated with the conversion of magnetic energy into kinetic and thermal energies after a rearrangement of magnetic field lines. Despite numerous studies on this subject, many aspects about magnetic reconnection remain unclear, in particular due to the

limited temporal resolution of instruments aboard past missions such as THEMIS [*Angelopoulos et al.,* 2008] and Cluster [*Escoubet et al.,* 2001]. The Magnetospheric Multiscale mission [*Burch et al.*, 2016] was launched on March 12, 2015. Its prime goal is the understanding of the microphysics of magnetic reconnection [*Burch and Phan*, 2016]. For that purpose, MMS is designed to provide unprecedented time resolution and measurement accuracy, which make the study of microscopic structures possible. The mission has allowed detailed studies of the electron diffusion region of magnetic reconnection, i.e., the smallest-scale region where even the electron motion decouples from the magnetic field [*Burch et al.*, 2016].

Complex magnetic structures can form at the magnetopause as a result of magnetic reconnection. Bursty and/or patchy magnetic reconnection may lead to the formation of flux transfer events (FTEs) on the dayside magnetopause [*Russell and Elphic*, 1978; 1979; *Hasegawa et al.,* 2006]. The two prime signatures of FTEs observed in situ are: (1) an enhancement in the magnetic field magnitude and (2) a bipolar signature in the component of the magnetic field normal to the magnetopause. A mixture of magnetosheath and magnetospheric ion and electron populations is often detected within FTEs [*Le et al.,* 1999]. FTEs have been studied using simulations [*Fedder et al.,* 2002; *Raeder,* 2006; *Daum et al.,* 2008], laboratory experiments [e.g., *Stenzel & Gekelman,* 1979; *Yamada,* 1999; Egedal et al., 2007; Fox et al., 2017], ground measurements [*Wild et al., 2*001*; Lockwood et al.,* 2001a, 2001b], and multi-spacecraft missions as Cluster [E.g. *Sonnerup et al.,* 2004; *Fear et al.,* 2005; *Hasegawa et al.,* 2006; *Roux et al.,* 2015], THEMIS [*Fear et al.,* 2009; *Silveira et al.,* 2012] and now MMS [*Farrugia et al*., 2016; *Hwang et al.*, 2016]. FTE models can essentially be classified into three types of models: elbow-shaped flux rope model [*Russell and Elphic*, 1978], multiple X-line model [*Lee and Fu,* 1985] and single X-line model [*Southwood et al.,* 1988; *Scholer,* 1988a; *Fear et al.,* 2008]. The properties and structure of FTEs have been the subject of many studies [*e.g. Scholer,* 1988*; Southwood et al.,* 1988*; Raeder et al.,* 2006*; Fear et al.,* 2008*; Fear et al.,* 2017].

Multi-spacecraft missions have advanced the understanding of FTEs shape, motion, and extent [*e.g. Fear et al.,* 2009*; Trenchi et al.,* 2016]. However, despite the abundance of FTE observations, their formation mechanism is not fully understood yet. More studies are still needed to better understand the detailed structure of FTEs and to link the observed properties to those at the formation site. The magnetic field topology within FTEs and their 3D magnetic

structure have also not been completely elucidated. Aside from large-scale FTEs often observed at the magnetopause, small-scale perturbations with magnetic signatures akin to those of FTEs might indicate the existence of very localized magnetic island structures [*Hesse et al.,* 1990]. Such magnetic islands may also be generated by multiple X-line reconnection [*Zhong et al.,* 2013; *Pu et al.,* 2013] (i.e., between two X-lines created sequentially on the magnetopause) or at a single X-line owing to rapid variations of the reconnection rate [*Huang et al.,* 2014]. Their typical signatures are an enhancement of the total magnetic field strength and a magnetic bipolar signature [*Teh et al.,* 2010]. In addition, plasma density dips have been reported at their center [*Zhou et al.,* 2014]. The core region is bounded by an electric current loop mainly carried by electrons [*Zhou et al.,* 2014]. The coalescence of magnetic islands, which corresponds to the merging of two islands into a larger one, has been observed in simulations [*Drake et al.,* 2006a; *Oka et al.,* 2010; *Zhou et al.,* 2014; *Huang et al.,* 2014]. Series of magnetic islands at the magnetopause have been reported [*Eastwood et al.,* 2007; *Teh et al.,* 2010; *Song et al.,* 2012]. During the coalescence of magnetic islands, a secondary magnetic reconnection process occurs at the interface of the two islands [*Pritchett,* 2008]. The compression associated with the coalescence leads to the formation of localized current sheets. *Øieroset et al.* [2016] reported MMS observations of magnetic reconnection in a compressed current sheet between colliding jets at the center of a flux rope. Those observations were quite similar to the one that will be further discussed in the present paper. In their paper, they concluded that the reconnection observed at the thin current sheet inside the flux rope was not consistent with coalescence of two flux ropes. Instead, they suggested that reconnection was 3D such that field lines did not form closed loops. Observations of magnetic flux ropes flanked by two X-lines between two converging jets were first reported by *Hasegawa et al.* [2010] and *Øieroset et al.* [2011].

The direct observation of complex 3D magnetic structures resulting from multiple X-line reconnection at the magnetopause have been also reported [e.g. *Øieroset et al*., 2011*, Zhong et al.*, 2013*; Pu et al.*, 2013]. Multiple X line magnetic reconnection occurs when magnetic reconnection takes place along several X-lines at the Magnetopause. The model by *Lee and Fu* [1985] explains the complex geometrical properties of FTEs. The occurrence of reconnection at multiple sites may imply reconfigurations of the magnetic field into a complex 3D magnetic topology. This may thus create complex 3D structures such as FTEs or other structures, some of which have been interpreted as interlaced magnetic flux tubes [*Louarn et al.,* 2004; *Cardoso et*

al., 2013]. For example, *Zhong et al.* [2013] showed that both open and closed field lines can coexist inside the central region of the FTE flux ropes. They considered this observation as a characteristic feature of 3-D reconnected magnetic flux ropes resulting from multiple, sequential x-line reconnection (MSXR). In this model, FTEs are generated by multiple X-line reconnection where new X-lines form sequentially [*Raeder et al*., 2006]. Furthermore, in *Pu et al*. [2013], electron energy-pitch angle distributions were used to infer the magnetic topology of field lines within an FTE. They found that the FTE was composed of flux ropes of four different magnetic topologies which indicates that the field lines must have reconnected multiple times. The coexistence of four different magnetic topologies was interpreted as the distinguishing feature of intrinsically 3D multiple X-line reconnection.

In this paper, we analyze an event which looks like a typical FTE at first sight. After detailed analysis we interpret the event as a current sheet resulting from the interaction of two converging and interlaced flux tubes. A similar interpretation has been suggested by *Louarn et al.* [2004] based on Cluster observations for an event that was observed on June 30, 2001, around 05:30 UT. They suggested a complex 3D topology resulting from the inter-linking of two magnetic flux tubes produced by two separate magnetic reconnection sites. They showed that the core fields of the two interacting and converging flux tubes had distinct orientations. The detailed interaction between the two flux tubes was not completely understood, however, owing to the limited time resolution of Cluster instrumentation. For the event considered in this paper, we show evidence for magnetic reconnection at the thin current sheet separating the two flux tubes, which was not observed for the event of *Louarn et al.* [2004].

We use the measurements from MMS spacecraft to study an event that was observed on 7 November 2015. We use ion and electron data from the Fast Plasma Investigation (FPI) instrument [*Pollock et al.*, 2016], ion composition data from Hot Plasma Composition Analyzer (HPCA) [*Young et al.*, 2016], and magnetic field from the fluxgate magnetometer (FGM) [*Russell et al.*, 2016; *Torbert et al.*, 2016]. We first discuss whether the event can be considered as an FTE or not. The structure of a thin current sheet encountered by MMS in the center of the event is analyzed in details. We interpret the presence of this current sheet inside the event as a result of the collision of two converging flux tubes.

2 Context

Figure 1a shows the interplanetary magnetic field (IMF) from OMNI [*King et Papitashvilie,* 2005] data over a few days surrounding the event. The period of interest, centered around 14:00 UT on 7 November 2015, occurred during the passage of a magnetic cloud at Earth. The magnetic cloud speed led to the formation of a shock in the solar wind, observed at 18:13 UT on November 6, followed by a corresponding sheath, which lasted until ~8:00 UT on November 7. Panels 1c-e in Figure 1 show the magnetic field, dynamic pressure and Alfvén Mach number zoomed in around the time of interest, during the first part of the magnetic cloud when its magnetic field had strong southward and dawnward components. The MMS event that was observed around 14:00 UT on November 7, occurred during a period of both strong driving of the magnetosphere (Dst = -69 nT, k_p=4) and low Alfvén Mach number (< 3). Under these conditions, solar wind-magnetosphere interaction is expected to be altered affecting in particular the flows in the magnetosheath uncommonly enhanced and distributed, the magnetopause shape and magnetic reconnection factors [see *Lavraud and Borovsky*, 2008].

Around 14:00 UT on November 7 (third dashed line in Figure 3), the MMS spacecraft were located in the dusk sector near the magnetopause. As illustrated in Figure 2, their barycenter was located at (8.6, 6.2, -0.9) R_E in GSE coordinates. Separated by about 10 km, they were in a good tetrahedron configuration with a quality factor of 0.84 [*Fuselier et al.*, 2016], which is suited for applying multipoint spacecraft methods [*Dunlop and Woodward,* 2000] as used in this study.

Two hours of MMS survey data are presented in Figure 3. The panels (a) to (g) show respectively, in GSE coordinates, the magnetic field components andtotal field strength, the electron and ion density, the ion velocity components and amplitude, the electron, ion, He^{2+}, and O^+ energy spectrograms. Initially, the spacecraft were located in the magnetosheath, as shown in the ion and electron spectrograms typical of the magnetosheath, high plasma number densities, and the abundance of He^{2+} and the absence of O^+ ion fluxes. After 14:28 UT, the spacecraft were inside the magnetosphere characterized by a positive and dominant B_Z, low number densities and weak flows, as well as high fluxes of observed energetic electrons, protons, and oxygen ions. Conversely, the He^{2+} fluxes were weak.

Around 13:28 UT, the data show a partial crossing of the magnetopause, as indicated by variable B_Z component and flows. We suspect that the sudden magnetopause crossing (i.e. magnetopause expansion) was produced by the arrival of the solar wind discontinuity that separates a high Mach number solar wind from low Mach number solar wind, as observed in the OMNI data around that time in Figure 1e. From then on, the prevailing solar wind has a low Mach number. Soon thereafter (~13:35 UT) the spacecraft exited back into the magnetosheath, as seen from the faster flows, similar to the previous magnetosheath interval. This magnetosheath interval was characterized by a much lower density and included two very short incursions into the magnetosphere. The main magnetopause crossing then occurred at 13:44:30 UT (second dashed line in figure 3). The boundary layer inside the magnetopause, hereafter called LLBL (for low latitude boundary layer), was observed from 13:44:30 UT to 14:00 UT. This LLBL interval was also very dynamic. This interval is identified as the outer LLBL because it contains plasma accelerated through the magnetopause discontinuity (marked by the magnetic field rotation), as evidenced by the enhanced and diverted flows as compared to the pristine magnetosheath observed before 13:45 (cf. panels a and c). The spacecraft entered more clearly into the

magnetosphere around ~14:00 UT where a second magnetic field rotation occurred, this time mainly in the B_Y component. We note that after this second current sheet the spacecraft did not exit immediately into the pristine magnetosphere given the observation of low energy magnetosheath electrons between 14:00 and 14:05 UT, reminiscent of a kind of, or a more inner part of, the LLBL. The true hot magnetospheric plasma was observed for example around 14:10 UT. The spacecraft exited back into the main (outer) LLBL with enhanced flows and negative B_Y around ~14:12 UT just before the event of interest, which was observed between 14:16:00 and 14:17:30 UT. The event time interval is indicated with a yellow shaded area, bracketed by the red vertical lines. A strong peak in magnetic field magnitude consists of the most spectacular feature and is visible in Figure3-a. Just after the event, the spacecraft remain in the LLBL based on the presence of some low energy magnetosheath electrons, but again likely the more inner part of it given the measured low densities and the positive B_Y value. The spacecraft are in the magnetosphere proper after around 14;28 UT (some middle energy electrons are intermittently observed after that time, but these are believed to be of ionospheric origin).

To summarize, we believe that two kinds of LLBL were present, as has been reported previously (e.g. *Hasegawa et al.,* 2003). The outer LLBL had a high density and showed enhanced $|V_Z|$ flows consistent with the passage through the magnetopause current sheet, which is characterized by a rotation of the magnetic field (B_Z increase) as well. The inner LLBL had, on the other hand, a lower density and a magnetic field orientation more consistent with the geomagnetic field observed in the pristine magnetosphere. The transition from the main (outer) LLBL to the inner LLBL also corresponded to a current sheet responsible for the main rotation in B_Y.

3 Data analysis

3.1. Large-scale structure

The crossing of the magnetopause and LLBL occurred between 13:44:30 UT and 14:00 UT. The magnetopause normal and associated LMN frame [*Farrugia et al*., 1988] were inferred by performing a variance analysis [*Sönnerup & Scheible*, 1998] of the magnetic field data between 13:42:25 and 14:02:44 UT. The results are given in table 1. The magnetopause normal vector (N = [0.84, 0.30, -0.44] in GSE) was relatively close to the normal direction calculated

from magnetopause models (e.g. [0.91, 0.41, -0.06] in GSE using the *Shue et al.* [1997] model). The L and M vectors roughly pointed in the Z and -Y directions.

In Figure 4, 100 seconds of burst data measured by MMS 1 are presented. Dashed lines labelled T_0 to T_5 delimit the different parts of the event that clearly have different properties and correspond to times 14:16:04; 14:16:25; 14:16:40; 14:16:43; 14:16:58 and 14:17:04.5 UT, respectively. The vector data are in GSE coordinates. The top panel (a) displays the magnetic field, the (b) panel the ion thermal pressure (P_p) , the magnetic pressure (P_m) and the total pressure ($Pt = P_p + P_m$). The (c) panel shows the current density as inferred from the curlometer technique, the (d) and (e) panels exhibit the ion velocity and the density of both ions and electrons. Electron data for the same interval are displayed in Figure 5. The second panel in Figure 5 shows the omnidirectional energy flux of electrons, and the following three panels (c, d, e) give the electron pitch-angle distributions for three energy ranges: 98-127 eV, 451-575 eV, and 3.3-11.5 keV. These energy bands are considered typical of thermal magnetosheath, accelerated magnetosheath and magnetospheric electron populations, respectively (e.g. *Pu et al.,* 2013, *Zhong et al.,* 2013). The top panel (a) displays the magnitude and By component of the magnetic field for the sake of completeness.

Figure 4 shows that prior to T_1 (14:16:25 UT), the spacecraft were in the inner LLBL, where plasma densities were low and B_Z was the main component of the magnetic field. Then, between T_1 and T_5, the MMS spacecraft recorded large changes in all parameters. The most remarkable features included peaks in the magnitudes of the magnetic field (by a factor of ~ 1.7) and total pressure (~2.5), a strong bipolar signature in the B_Y component ($\Delta B_Y \sim 80$ nT) and a large (~300 km/s) flow directed northward ($V_Z > 0$) and eastward ($V_Y > 0$). At first glance, these large-scale signatures are consistent with those of an FTE consisting of a flux rope resulting from a reconnection process, that may have occurred southward and dawnward of the spacecraft for the prevailing conditions of IMF negative B_Z and B_Y (see Figure 1).

This interpretation appears, however, inconsistent with several observational facts. (i) First, the bipolar signature was not observed in the component normal to the magnetopause (mainly along X_{GSE}), but rather in a direction almost perpendicular (B_{YGSE}) to the magnetopause normal (see Panel a). (ii) Secondly, there were a small-scale and fast $V_Y = 300$ km/s ion jet (along Y_{GSE}) and an intense and thin current structure near the peak of the large scale magnetic field between T_2 and T_3 (Panels d, c and a). Such features do not fit the usual flux rope models of

FTEs, although the presences of thin current sheets and reconnection have been reported in the literature [*Øieroset et al.*, 2016]. (iii) Thirdly, based on the pitch-angle distribution of electrons, there were drastically different regimes before and after the passage of this current structure (last three panels in Figure 5). The characteristic features of the first and second part of the event were clearly different. The region between T_1 and T_2 was first characterized by lower fluxes of anti-parallel accelerated magnetosheath electrons, while the parallel fluxes remained unchanged with regards to the fluxes measured before T_1 (Panel d). On the other hand, the thermal magnetosheath electron population tended to have larger fluxes, consistent with an increased density (Panel c). During this interval, MMS also observed a trapped electron population (at 90° pitch angle) which appears in both the accelerated magnetosheath and magnetospheric energy ranges (Panels d and e). By contrast, during the second part of the event (between T_3 and T_4), this trapped population was not present anymore; there were essentially no magnetospheric electrons. The accelerated magnetosheath electrons anti-parallel flux was larger than the parallel one (Panel d). These strongly different features suggest that this sequence is not the signature of a single homogenous structure like a flux rope (expected to be associated with FTEs). We rather interpret the time sequence between T1 and T4 as successive crossings of two distinct flux tubes, henceforth referred to as FT_A (T1-T2) and FT_B (T3-T4). Finally, the densities were also drastically different between FT_A and FT_B (Figure 4, Panel e). In FT_B, the electron/ion densities and the He^{2+} fluxes (Figure 2) had values typical of the outer LLBL.

A complementary view is provided in Figure 6 that introduces our observations in the LMN frame. The components of the magnetic field are shown in panels a to d. The ion velocity components are provided in panels f to l and the angle Ψ is shown in panel e. Ψ is the angle between the magnetopause normal and the magnetic field ($\Psi = \text{atan}\{(B_L^2 + B_M^2)^{1/2} / |B_N|\}$). Displaying the data in the LMN frame reveals two main features at the scale of the whole event: (i) the magnetic changes in the LMN frame did not exhibit an FTE-like bipolar signature, but rather a sharp rotation of the magnetic field through a thin current structure. The maximum magnetic field shear angle, corresponding to that across the central thin current sheet, was about 73°. Before its passage, the magnetic field was progressively deformed throughout T_0-T_1-T_2, as indicated by the gradual changes in Ψ. When the spacecraft crossed the current structure, the Ψ angle recovered quickly its initial value and, thereafter, both the L and N components of the magnetic field remained close to zero for about 15 seconds, while the M-component was

strongly enhanced. (ii) The event was associated with a perpendicular ion flow in the +L direction, suggesting that reconnection occurred southward of the spacecraft.

A more detailed examination of the observations indicates that at the beginning of the period, before T_0, the magnetic field had an orientation tangential to the magnetopause, mainly in the L direction. The Ψ angle was close to 90°. The ion flows were weak. At time T_0, while all other parameters remained unchanged, the Ψ angle (B_N component) started to decrease (increase). This trend continued until T_1 and indicates that the magnetic field underwent a large-scale deformation. This is interpreted as the remote signature of a propagating process having started before T_0 and approaching closer to the spacecraft. During this period, the ion flow remained constantly weak (V_{iL} ~-50 km/s, V_{iM} ~-25 km/s) except for a small V_N (also seen on the V_{XGSE} component) peak ~5 seconds prior to T_1. This V_N change consisted of a perpendicular flow and was negative indicating an inward motion of plasma. This one could be due to a local retreat of the magnetopause. The time T_1 marks the beginning of the in-situ detection of the event, corresponding to the entry into flux tube FT_A. Between T_1 and T_2, the B_L component and the magnitude of the magnetic field both increased. It was also the general trend for B_N while B_M decreased to ~15 nT. When the spacecraft penetrated into FT_A (at T_1), it first detected a ~3 second duration anti-parallel ion flow that reached a maximum value of 150 km/s along the L and N directions. Then, when V_L and V_N returned to zero, the flow was mainly perpendicular with a $-V_M$ component. From that time until T_2 (14:16:40 UT), the main component of the flow was $-V_M$, suggesting a westward motion of FT_A.

Between T_2 and T_3, the magnetic field rapidly rotated. A localized ion jet was detected at that time, as clearly seen on the V_{YGSE} component in Figure 4. This jet appeared in the L and M components in Figure 6. It was thus directed in a direction tangential to the magnetopause and oblique to the magnetic field as it includes both parallel and perpendicular components. Comparison to the electric field data (not shown) indicates that the ions were decoupled from the magnetic field during the main current structure. Being along V_M during a large rotation of the B_M component, this ion jet is consistent with expectations from magnetic reconnection between FT_A and FT_B, as is discussed later.

Between T_3 and T_4, the flow was essentially along the L direction and the N and L components of magnetic field were close to zero.

Finally, between T_4 and T_5, the ion flow vanished gradually and the magnetic field recovered its initial (before T_0) orientation. The interface marking the end of the event is not analysed in further detail in this paper.

3.2. Small-scale current sheet

In order to infer the motion of the current structure relative to the spacecraft, we performed differential timing analysis using the B_{YGSE} bipolar transition, which constitutes the clearest change. This transition corresponded to the crossing of a strong current structure. We identified times when the 4 MMS spacecraft successively measured a set of identical B_Y values, as illustrated in Figure 7 with the horizontal dashed lines. Assuming that the structure is planar, we applied the multi-point triangulation method [*Russell et al.*, 1983, *Harvey et al.*, 1998]. For all identified times it provided a set of normal vectors $\mathbf{N_C}$ and propagation speed V_P along the normal. The results showed that both N_C and V_P change only slightly through the transition. From now on we thus use a normal vector $N_C = [-0.5456; -0.0308; 0.8375]_{GSE}$ and a propagation velocity of ~67 km/s, which are obtained from averaging over the full set of values shown in Table 2.

For inferring the geometry and the orientation of the current structure, we performed the variance analysis of the current density measurement obtained with the curlometer technique [*Robert et al.,* 1998] for the period 14:16:39 – 14:16:43 UT. The results given in Table 3 exhibit a strong contrast between the eigenvalues and thus indicate that the current structure was organized wih respect to clearly defined principal axes. The axis of maximal current (called thereafter "main current") was directed in the $(–X,-Z)_{GSE}$ direction [-0.76, -0.20, -0.61]. The second principal axis associated with a significant (λ_1/λ_2 ~2.8) current contribution (called thereafter "secondary current") was close to the Y_{GSE} direction [0.03, -0.96, 0.28]. The third principal axis was associated with much lower eigenvalue (λ_2/λ_3 ~15.43) with an almost null current component. Its orientation [-0.65, 0.19, 0.74] was in the $(–X, +Z)_{GSE}$ direction and was found to be close to the direction of N_C found from the differential timing analysis.

Both independent approaches (current variance analysis and triangulation method) thus provided a consistent geometry of the current structure. We then considered a new coordinate system referred thereafter as the PCS (Propagation Current Structure) frame, which is illustrated in Figure 8. The PCS coordinate system is defined by the vectors $\vec{U}_P$, $\vec{U}_J$ and $\vec{U}_V$. The

components of these unit vectors in the GSE frame are shown in Table 4. The first unit vector [-0.6124; 0.0239; 0.7902] $_{GSE}$ is close to the propagation direction as well as the normal direction of the current structure. The second axis is chosen to be a direction opposite to the main current [0.7676; -0.2209 ; 0.6016]$_{GSE}$ and the last axis is defined using the unit vector of the ion jet which is also close to the unit vector of the secondary current [0.1889; 0.9750; 0.1169]$_{GSE}$ (almost coinciding with Y_{GSE}). In order to follow the current structure, the PCS frame is in translation relatively to the GSE one at a translation velocity equal to the propagation velocity derived from the differential timing analysis.

The Figure 9 shows data coming from the FGM and FPI experiments onboard MMS-1 for a 6-second period including the current structure observation. The GSE coordinates of the current density (from curlometer technique) are represented in panel (a). A correlation between J_X and J_Z is clearly visible and J_Y exhibits a bipolar signature. As showed in panel (b) the current was mostly parallel to the magnetic field. In panel (c), the magnitudes of the current density obtained from the curlometer technique J_{curl} (FGM data) and the ones directly computed from the particle measurement (FPI data) are compared. J_i (green) is the ion current, J_e (blue) the electron current and J_{part} is obtained from $ne(V_i - V_e)$. It appears clearly that the current was carried by the electrons while the ion contribution was almost negligible.

The panel (d) displays the current density (from the curlometer technique) in the PCS frame. The spacecraft reached the structure around 14:16:39.70 UT (time marked by the first black dashed vertical line) as indicated by the little jump seen on J_J, J_V and $J_{//}$. Then, the satellites recorded a gradual increase (in absolute value) of the main current component and a sharp peak between 14:16:40.96 UT and 14:16:41.54 UT (times indicated by the red vertical lines). Eventually, MMS-1 exited out of the current structure around 14:16:42.22 UT (time marked the second black dashed vertical line). Encircling the main current peak, a bipolar secondary current was measured.

Multiplying the 2.52 s duration of the current structure crossing (interval between the pair of black dashed vertical lines in Figure 9) with the propagation velocity, we find that the spatial scale of the entire current structure is about 169 km. This is about 3 times the ~60 km Larmor radius of thermal protons at the time of the current sheet encounter. The crossing of the main current peak, as indicated between the two vertical redlines in Figure 9, lasted 0.58 seconds,

which corresponds to ~39 km. That is, the dimension of the main current peak was smaller than the proton Larmor radius.

The panel (e) shows the PCS magnetic field components. We note that the B_P changes remained very small. Similarly, B_J was also roughly constant except a peak correlated with the main current one. The B_J peak is consistent with the bipolar secondary current. The main change of the magnetic field was on the B_V component suggesting that the main current (along the J-direction) consisted of a current sheet oriented along the V-direction.

The panel (f) displays the ion velocity in the PCS frame. The ion jet is seen as a peak now on the V-component taking place between the first black dashed vertical line and the second red vertical line. The ion jet crossing lasted for ~1.8 seconds. Multiplying by the propagation velocity, this gives a thickness of 120 km, corresponding to ~2 proton Larmor radii. We note that the ion jet was observed concomitant with the overall current structure, but that the current peak took place on its downstream side relatively to the structure propagation, i.e., when the main flow component (V_{iV}) was decreasing (panel g).

The ion flow velocity is displayed at a larger scale, and in the PCS frame in panel (g) of Figure 9. The V_{iP} component along the propagation direction, which also corresponds to the normal to the current sheet, showed a clear reversal upon crossing the current structure. V_{iP} was first negative, indicating that the plasma moved slower than the current structure in the propagation direction. After the current sheet and ion jet (observed in V_{iV}), it was positive, and the ions moved faster. This means that in the PCS frame (i.e. in the frame moving with the current structure) the flows were converging toward the current structure, which thus was being compressed by the surrounding plasma. There was also a flow reversal along the main current direction, as indicated by the reversal in the V_{iJ} component. This suggests that there was also a flow shear along the current structure, in addition to the compression. Around 14:17:05-14:17:10 UT, i.e. just after T5, all flow components reversed. This is interpreted as indicating that the spacecraft re-entered into the inner LLBL.

4 Discussion and interpretation

4.1 Phenomenological interpretation

The event analyzed in this study exhibits some features apparently similar to FTEs at first glance, i.e. bipolar variation of a magnetic field component and a peak in the magnetic field

strength. However, a more detailed examination showed that it cannot be interpreted as a single FTE entity consisting of a single helicoidal flux tube. The main reasons are the following: (i) The bipolar change in the magnetic field did not occur in the expected direction normal to the magnetopause, (ii) A strong and thin current structure and a localized ion jet, were detected near the center, and (iii) The electron pitch-angle distributions indicate that the event did not consist of a unique and homogenous structure with a single connectivity as expected for a large-scale flux rope. Before proposing an alternative interpretation, let us first summarize the main features of the event. Times T_0 to T_5 mentioned below refer to the vertical dashed lines in Figures 4, 5 and 6.

- The event took place during the passage of an interplanetary magnetic cloud. The IMF was intense and stable, with all three GSE components being negative. The solar wind pressure and the Alfvén Mach number were very low.
- The event occurred when the spacecraft were in the Low Latitude Boundary Layer (LLBL).
- $T_0 \rightarrow T_1$: The first signature consisted of a change in the magnetic field only, suggestive of remote sensing of the structure propagating toward the spacecraft.
- $T_1 \rightarrow T_2$: The spacecraft entered a flux tube (FT_A) mainly characterized by accelerated magnetosheath electrons exhibiting an anisotropy in the direction parallel to the magnetic field. Moreover, trapped magnetospheric electrons were continuously measured in FT_A. The density was slightly enhanced and B_{YGSE} was positive. Ions first streamed antiparallel to the magnetic field and then perpendicular in the duskward (Y_{GSE} or -M) direction. A trapped population of suprathermal electrons was continuously measured in this flux tube.
- $T_3 \rightarrow T_4$: In the second part of the event, the spacecraft crossed a very different flux tube (FTB). There was no trapped electron population and the anisotropy of the accelerated magnetosheath was in the opposite sense, in the antiparallel direction. B_{YGSE} was the main component of the magnetic field and was negative. The density was higher with values close to the ones measured inside the outer LLBL, between 13:45 and 14:00 for example. The plasma flow was in the northward and duskward direction.

- $T_2 \rightarrow T_3$: Between these two flux tubes, there was a strong and thin current sheet where the magnetic field rotated sharply. A strong and localized duskward ion jet along the Y_{GSE} direction was also observed, qualitatively consistent with a reconnection process occurring inside the current sheet owing to the sharp B_Y reversal. In the frame moving with the structure the surrounding plasma flow was converging towards the current sheet. The current sheet was thus being compressed.

We interpret this sequence of observations as the signature of the successive crossing of the two flux tubes by the spacecraft. These two flux tubes may have been generated by multiple sequential reconnection process, which is expected to occur under strong BY and negative BZ IMF conditions, as was observed for a long time around the event [e.g. Raeder, 2006; Pu et al., 2013]. The first flux tube (FTA) contained trapped electrons. This implies that this flux tube has a different history and connectivity compared to the second flux tube which rather contained only magnetosheath electrons with largely different pitch angle properties [Pu et al., 2013]. A current sheet formed at the interface between the two flux tubes. As shown by the changes in the ion velocity component along the propagation direction (Figure 8-g), the second flux tube (FTB) was moving faster than the first one (FTA). This resulted in an interlaced magnetic structure and associated complex 3D topology, as has been previously studied with Cluster data [Louarn et al., 2004]. The observed compression is likely at the origin of the current sheet formation and of the reconnection occurring inside as described next.

4.2. Reconnection at the thin current sheet

Reconnection driven by compression at current sheets formed by the interaction of plasma flows have been suggested for interpreting spacecraft observations from the magnetopause [*Øieroset et al.,* 2016], in the magnetotail [*Alexandrova et al.*, 2016] and simulation results as well [*Oka et al*., 2010, *Huang et al.*, 2014]. Simulations have been performed in particular to study the coalescence of magnetic islands, and showed features similar to the ones identified in this event. This is true, in particular, for the formation of a thin current sheet with an exhaust in the transverse direction [*Zhou et al.,* 2014].

Qualitatively, the local conditions satisfied at the interface of coalescing magnetic islands are somewhat similar to those observed in our event. Locally, this corresponds to the interaction

between two disconnected magnetic flux tubes pushed against one another by the differential plasma flows in which they are imbedded. MMS measurements thus permit a detailed analysis of such a case, but with some conditions specific to the event: the current sheet was characterized by a large density jump and a magnetic shear angle of only ~73° as compared with 180° in published simulations with comparable densities [*Galsgaard et al.,* 2000].

Figure 10 shows a sliced schematic view of the crossing in the PCS frame. The spacecraft started in the low density flux tube FT_A at T_1. The V component of the magnetic field was positive inside FT_A. An ion jet, as represented by red arrows with a yellow outline, was observed inside the current sheet (which is about 169 km thick). At the second edge of the jet, the spacecraft crossed a complex current structure (between T_2 and T_3). It consisted of a strong and peaked current sheet directed in the $\overrightarrow{-\mathbf{U_J}}$ direction encircled by a pair of current sheets of opposite polarities along the $\vec{\mathbf{U}}_\mathbf{V}$ direction. Between T_3 and T_4, the spacecraft were in FT_B, where the V component of the magnetic field is negative. The combined effect of opposite (bipolar) currents as observed in the $\vec{\mathbf{U}}_\mathbf{V}$ direction was to produce an enhancement of the positive B_J component in between them (as represented by the green arrows). In doing so, these currents directly supported the rotation of the magnetic field from the FT_A to the FT_B orientations. This enhancement in the B_J component is clearly seen in Figure 9f as a 15~20 nT peak superimposed on top of the larger-scale constant $B_\mathbf{J}$ ~50 nT. The red vectors in the $\pm\vec{\mathbf{U}}_\mathbf{p}$ directions illustrate the compression of the current structure by two oppositely-directed flows (which converge toward it).

The process at the origin of the ion jet observed inside the first current sheet was likely magnetic reconnection driven by the compression of the two distinct sets of open field lines. This is partially supported by the Walén test results that are superimposed on the main jet velocity component in figure 9g. Walén tests [e.g. *Phan et al.*, 2004] were performed with positive and negative correlations on the Earthward (upstream relative to the structure propagation) and Sunward (downstream) sides of the exhaust, respectively. The exhaust was observed between 14:16:39.7 and 14:16:41.7 UT. This is presented in figure 9g with $V_{IONS} - V_{HT} = +/- V_A$, where V_{IONS}, V_{HT}, and V_A are the bulk ion, deHoffman-Teller and Alfvén velocity vectors, respectively. The Walén test would predict an ion jet with amplitude ~688 km/s. This is much larger than the

amplitude of the observed jet. The correlation coefficient is of -0.92 and the slope is of -0.68 for the entry to the exhaust between 14:16:39.7 and 14:16:40.95 UT. For the exit from the exhaust, between 14:16:40.95 and 14:16:41.7 UT, the Walén relation provides a correlation coefficient of 0.92 with a slope of 0.18, which is much lower than the ideal value ±1. Although the Walén test shows that the ion bulk flow is not as large as expected, this may be due to the proximity to the X-line [*Phan et al.,* 2016]. To support this hypothesis, we note that with densities of 2 and 6 cm^{-3}, as measured each side of the exhaust at 14:16:39.7 UT and 14:16:41.7 UT, the typical ion skin depth λ_i is estimated as 100-155 km. The jet thickness is thus estimated to be approximately 120 km, or about 0.8-1.3 λ_i. Such a thickness implies that we are very close to the X-line (5-8 λ_i or ~840 km), which is consistent with the ion jet not being fully developed yet and thus with the over-estimation of the ion speed from the Walén test.

5 Summary and conclusions

We have studied in detail what initially looked on face value like a classic FTE at the Earth's dayside magnetopause, as observed by the MMS mission. Due to its high-resolution measurements, our analysis revealed the following unusual properties:

- The large-scale magnetic field bipolar signature was not found in the component normal to the nominal magnetopause surface, but rather in the B_{YGSE} component;
- The densities and pitch angle distributions of suprathermal electrons shows that the current sheet separated two distinct plasmas with different properties and magnetic connectivities;
- An intense and complex current structure, supporting the large reversal in the B_{YGSE} component, was observed near the peak in the magnetic field strength;
- This current was carried by electrons. Although the scale of the structure is approximately three times the ion Larmor radius, the structure possesses smaller scale sub-structures, smaller than the ion Larmor radius. The intense current sheet was associated with a strong transverse flow (along V_{YGSE}) consistent with expectations from magnetic reconnection therein.

Our interpretation is that these properties are incompatible with a classic, single FTE structure. The data is rather consistent with a complex, three-dimensional interaction of two distinct flux tubes. This compressive interaction led to the formation of a thin and complex

current structure between two flux tubes of very different orientations (73° magnetic shear angle) which mimicked the bipolar magnetic structure and the enhanced core magnetic field, both expected for classic FTEs. The strong magnetic field pile-up and ensuing thin current sheet also appeared to have triggered magnetic reconnection at the interface.

Acknowledgments, Samples, and Data

We thank all the MMS teams and instrument PIs for data access and process. Work at IRAP was supported by CNRS and CNES. C.J.F work was partially supported by NASA grants 499878Q and NNX16AO04G. MMS data visualization and analysis was performed with the CL software (http://clweb.irap.omp.eu/). We used also AMDA science analysis system and 3DView visualization tool provided by the Centre de Données de la Physique des Plasmas (CDPP) supported by CNRS, CNES, Observatoire de Paris and Université Paul Sabatier, Toulouse (http://amda.irap.omp.eu/ and http://3dview.irap.omp.eu/). MMS data are available at https://lasp.colorado.edu/mms/sdc/public/.

References

Alexandrova, A., R. Nakamura,E. V. Panov, Yu. L. Sasunov,T. Nakamura, Z. Vörös, A. Retinò,and V. S. Semenov (2016), Twointeracting X lines in magne-totail: Evolution of collisionbetween the counterstreaming jets,Geophys. Res. Lett., 43, 7795–7803,doi:10.1002/2016GL069823.

Angelopoulos, V. "The THEMIS Mission." *Space Science Reviews* 141, no. 1–4 (December 1, 2008): 5. doi: 10.1007/s11214-008-9336-1.

Biernat H K. Coupling processes at the magnetopause. In: Biernat H K, Bauer S J, Heinder M, eds. Theoretical problems in space and fusion plasmas. Wien: Oesterreichischen Akademie der Wissenschaften, 1991. 105

Burch, J. L., T. E. Moore, R. B. Torbert, and B. L. Giles. "Magnetospheric Multiscale Overview and Science Objectives." *Space Science Reviews* 199, no. 1–4 (March 1, 2016): 5–21. doi:10.1007/s11214-015-0164-9.

Burch, J. L., and T. D. Phan (2016), Magnetic reconnection at the dayside magnetopause: Advances with MMS, Geophys. Res. Lett., 43, 8327 –8338, doi: 10.1002/2016GL069787.

Cardoso, F. R., W. D. Gonzalez, D. G. Sibeck, M. Kuznetsova, and D. Koga, Magnetopause reconnection and interlinked flux tubes, *Annales Geophysicae*, 31, 1853-1866, 2013, doi:10.5194/angeo-31-1853-2013.

Daum, P., J. A. Wild, T. Penz, E. E. Woodfield, H. RèMe, A. N. Fazakerley, P. W. Daly, and M. Lester. "Global MHD Simulation of Flux Transfer Events at the High-Latitude Magnetopause Observed by the Cluster Spacecraft and the SuperDARN Radar System." *Journal of Geophysical Research (Space Physics)* 113 (July 1, 2008): A07S22. doi:10.1029/2007JA012749.

Drake, J. F., M. Swisdak, H. Che, and M. A. Shay, Electron Acceleration from Contracting Magnetic Islands During Reconnection, Nature (London) 443, 553 (2006).

566 Dungey, J. W. "Interplanetary Magnetic Field and the Auroral Zones." *Physical Review Letters*
567 6, no. 2 (January 15, 1961): 47–48. doi:10.1103/PhysRevLett.6.47.

568 Dunlop, M. W., and T. I. Woodward, Discontinuity analysis: Orientation and motion, in Analysis
569 Methods for Multispacecraft Data, *ISSI Sci. Rep. SR-001*, p. 271, Kluwer Acad., Norwell,
570 Mass., 1998.

571 Dunlop, M. W., A. Balogh, K.-H. Glassmeier, and P. Robert. "Four-Point Cluster Application of
572 Magnetic Field Analysis Tools: The Curlometer." *Journal of Geophysical Research*
573 *(Space Physics)* 107 (November 1, 2002): 1384. doi: 10.1029/2001JA005088.

574 Eastwood, J. P., T.-D. Phan, F. S. Mozer, M. A. Shay, M. Fujimoto, A. Retinò, M. Hesse, A.
575 Balogh, E. A. Lucek, and I. Dandouras (2007), Multi-point observations of the Hall
576 electromagnetic field and secondary island formation during magnetic reconnection, *J.*
577 *Geophys. Res*., 112, A06235, doi: 10.1029/2006JA012158.

578 Eastwood, J. P., T. D. Phan, M. Øieroset, M. A. Shay, K. Malakit, M. Swisdak, J. F. Drake, and
579 A. Masters. "Influence of Asymmetries and Guide Fields on the Magnetic Reconnection
580 Diffusion Region in Collisionless Space Plasmas." *Plasma Physics and Controlled*
581 *Fusion* 55, no. 12 (2013): 124001. doi:10.1088/0741-3335/55/12/124001.

582 Egedal, J., W. Fox, N. Katz, M. Porkolab, K. Reim, and E. Zhang. "Laboratory Observations of
583 Spontaneous Magnetic Reconnection." *Physical Review Letters* 98, no. 1 (January 5,
584 2007): 015003. doi:10.1103/PhysRevLett.98.015003.Escoubet, C. P., M. Fehringer, and
585 M. Goldstein. "IntroductionThe Cluster Mission." *Ann. Geophys.* 19, no. 10/12
586 (September 30, 2001): 1197–1200. doi:10.5194/angeo-19-1197-2001.
587 Farrugia, C. J., D. J. Southwood, and S. W. H. Cowley. "Observations of Flux Transfer Events."
588 *Advances in Space Research* 8, no. 9 (January 1, 1988): 249–58. doi:10.1016/0273-
589 1177(88)90138-X.
590 Farrugia, C. J., B. Lavraud, R. B. Torbert, M. Argall, I. Kacem, W. Yu, L. Alm, et al.
591 "Magnetospheric Multiscale Mission Observations and Non-Force Free Modeling of a
592 Flux Transfer Event Immersed in a Super-Alfvénic Flow." *Geophysical Research Letters*
593 43 (June 1, 2016): 6070–77. https://doi.org/10.1002/2016GL068758.

594 Fear, R. C., A. N. Fazakerley, C. J. Owen, A. D. Lahiff, E. A. Lucek, A. Balogh, L. M. Kistler,
595 C. Mouikis, and H. Rème. "Cluster Observations of Bounday Layer Structure and a Flux
596 Transfer Event near the Cusp." *Ann. Geophys.* 23, no. 7 (October 14, 2005): 2605–20.
597 doi: 10.5194/angeo-23-2605-2005.

598 Fear, R. C., S. E. Milan, A. N. Fazakerley, E. A. Lucek, S. W. H. Cowley, and I. Dandouras.
599 "The Azimuthal Extent of Three Flux Transfer Events." *Ann. Geophys.* 26, no. 8 (August
600 5, 2008): 2353–69. doi:10.5194/angeo-26-2353-2008.

601 Fear, R. C., S. E. Milan, A. N. Fazakerley, K.-H. Fornaçon, C. M. Carr, and I. Dandouras.
602 "Simultaneous Observations of Flux Transfer Events by THEMIS, Cluster, Double Star,
603 and SuperDARN: Acceleration of FTEs." *Journal of Geophysical Research (Space*
604 Physics) 114 (October 1, 2009): A10213. https://doi.org/10.1029/2009JA014310.

605 Fear R.C*,* L. Trenchi*,* J.C. Coxon*, and* S.E. Milan *(*2017*),* How much flux does a flux transfer
606 event transfer?*,* J. Geophys. Res.*,* 122*, doi:*10.1002/2017JA024730*.*

Fedder, J. A., S. P. Slinker, J. G. Lyon, and C. T. Russell. "Flux Transfer Events in Global Numerical Simulations of the Magnetosphere." Journal of Geophysical Research: Space Physics 107, no. A5 (May 1, 2002): SMP 1-1. doi:10.1029/2001JA000025.

Fox, W., F. Sciortino, A. v. Stechow, J. Jara-Almonte, J. Yoo, H. Ji, and M. Yamada. "Experimental Verification of the Role of Electron Pressure in Fast Magnetic Reconnection with a Guide Field." Physical Review Letters 118, no. 12 (March 21, 2017): 125002. doi:10.1103/PhysRevLett.118.125002.

Fuselier, S.A., Lewis, W.S., Schiff, C. et al. Space Sci Rev (2016) 199: 77. doi: 10.1007/s11214-014-0087-x.

Galsgaard K., Parnell C. E., Blaizot J. 2000 Elementary heating events—magnetic interactions between two flux sources. Astron. Astrophys. 362, 395–405

1Harvey, C. C. (1998), "Spatial gradients and the volumetric tensor", in Analysis Methods for Multi-Spacecraft Data, edited by G. Paschmann and P. W. Daly, pp. 307–348, Int. Space Sci. Inst., Bern.

Hasegawa, H., M. Fujimoto, K. Maezawa, Y. Saito, and T. Mukai (2003), Geotail observations of the dayside outer boundary region: Interplanetary magnetic field control and dawn-dusk asymmetry, J. Geophys. Res., 108, 1163, doi:10.1029/2002JA009667, A4.

Hasegawa, H., B. U. Ö. Sönnerup, C. J. Owen, B. Klecker, G. Paschmann, A. Balogh, and H. Rème. "The Structure of Flux Transfer Events Recovered from Cluster Data." *Annales Geophysicae* 24 (March 2006): 603–18. doi:10.5194/angeo-24-603-2006.

Hasegawa, H., J. Wang, M. W. Dunlop, Z. Y. Pu, Q.-H. Zhang, B. Lavraud, M. G. G. T. Taylor, et al. "Evidence for a Flux Transfer Event Generated by Multiple X-Line Reconnection at the Magnetopause." *Geophysical Research Letters* 37, no. 16 (August 1, 2010): L16101. doi:10.1029/2010GL044219.

Hesse, Michael, Joachim Birn, and Karl Schindler. "On the Topology of Flux Transfer Events." *Journal of Geophysical Research: Space Physics* 95, no. A5 (May 1, 1990): 6549–60. doi:10.1029/JA095iA05p06549.

Huang, S. Y., M. Zhou, Z. G. Yuan, X. H. Deng, F. Sahraoui, Y. Pang, and S. Fu (2014), Kinetic simulations of electric field structure within magnetic island during magnetic reconnection and their applications to the satellite observations, J. Geophys. Res. Space Physics, 119, 7402–7412, doi: 10.1002/2014JA020054.

Hwang, K.-J., D. G. Sibeck, B. L. Giles, C. J. Pollock, D. Gershman, L. Avanov, W. R. Paterson, et al. "The Substructure of a Flux Transfer Event Observed by the MMS Spacecraft." *Geophysical Research Letters* 43 (September 1, 2016): 9434–43. https://doi.org/10.1002/2016GL070934.

King, J. H., and N. E. Papitashvili. "Solar Wind Spatial Scales in and Comparisons of Hourly Wind and ACE Plasma and Magnetic Field Data." *Journal of Geophysical Research (Space Physics)* 110 (February 1, 2005): A02104. https://doi.org/10.1029/2004JA010649.

Lavraud, B., and J. E. Borovsky (2008), "Altered solar wind-magnetosphere interaction at l ow Mach numbers: Coronal mass ejections", J. Geophys. Res., 113, A00B08, doi: 10.1029/2008JA013192.

Le, G., J. T. Gosling, C. T. Russell, R. C. Elphic, M. F. Thomsen, and J. A. Newbury. "The Magnetic and Plasma Structure of Flux Transfer Events." *Journal of Geophysical Research: Space Physics* 104, no. A1 (January 1, 1999): 233–45. doi:10.1029/1998JA900023.

Lee, L. C., and Z. F. Fu. "A Theory of Magnetic Flux Transfer at the Earth's Magnetopause." *Geophysical Research Letters* 12, no. 2 (February 1, 1985): 105–8. doi:10.1029/GL012i002p00105.

Lemaire J, Roth M. Penetration of solar wind plasma elements into magnetoshere. J Atmos Terr Phys, 1978, 40: 331.

Lockwood, M., Fazakerley, A., Opgenoorth, H., Moen, J., van Eyken, A. P., Dunlop, M., Bosqued, J.-M., Lu, G., Cully, C., Eglitis, P., McCrea, I. W., Hapgood, M. A., Wild, M. N., Stamper, R., Denig, W., Taylor, M., Wild, J. A., Provan, G., Amm, O., Kauristie, K., Pulkkinen, T., Stromme, A., Prikryl, P., Pitout, F., Balogh, A., Reme, H., Behlke, R., Hansen, T., Greenwald, R., Frey, H., Morley, S. K., Alcayde, D., Blelly, P.-L., Donovan, E., Engebretson, M., Lester, M., Watermann, J., and Marcucci, M. F.: Coordinated Cluster and ground-based instrument observations of transient changes in the magnetopause boundary layer during an interval of predominantly northward IMF: Relation to reconnection pulses and FTE signatures, Ann. Geophys., 19, 1613–1640, 2001a.

Lockwood, M., Opgenoorth, H., van Eyken, A. P., Fazakerley, A., Bosqued, J.-M., Denig, W., Wild, J. A., Cully, C., Greenwald, R., Lu, G., Amm, O., Frey, H., Strømme, A., Prikryl, P., Hapgood, M. A., Wild, M. N., Stamper, R., Taylor, M., McCrea, I., Kauristie, K., Pulkkinen, T., Pitout, F., Balogh, A., Dunlop, M., Reme, H., Behlke, R., Hansen, T., Provan, G., Eglitis, P., Morley, S. K., Alcayd, D., Blelly, P.-L., Moen, J., Donovan, E., Engebretson, M., Watermann, M. L. J., and Marcucci, M. F.: Coordinated Cluster, ground-based instrumentation and low-altitude satellite observations of transient poleward-moving events in the ionosphere and in the tail lobe, Ann. Geophys., 19, 1589–1612, 2001b.

Louarn, P., A. Fedorov, E. Budnik, G. Fruit, J. A. Sauvaud, C. C. Harvey, I. Dandouras, H. Rème, M. C. Dunlop, and A. Balogh. "Cluster Observations of Complex 3D Magnetic Structures at the Magnetopause." *Geophysical Research Letters* 31, no. 19 (October 1, 2004): L19805. doi:10.1029/2004GL020625.

Pu, Z. Y., J. Raeder, J. Zhong, Y. V. Bogdanova, M. Dunlop, C. J. Xiao, X. G. Wang, *and* A. Fazakerley *(*2013*),* Magnetic topologies of an in vivo FTE observed by Double Star/TC-1 at Earth's magnetopause*, Geophys. Res. Lett.,* 40*,* 3502–3506*, doi:*10.1002/grl.50714.

Raeder, J.: Flux Transfer Events: 1. generation mechanism for strong southward IMF, Ann. Geophys., 24, 381-392, doi: 10.5194/angeo-24-381-2006, 2006.

Robert, P., M. W. Dunlop, A. Roux, and G. Chanteur (1998), Accuracy of current density determination, in Analysis Methods for Multi-Spacecraft Data, edited by G. Paschmann and P. W. Daly, p. 395, ESA Publ., Noordwijk, Netherlands. Roux, Alain, Patrick Robert, Dominique Fontaine, Olivier Le Contel, Patrick Canu, and Philippe Louarn.

"What Is the Nature of Magnetosheath FTEs?" *Journal of Geophysical Research: Space Physics* 120, no. 6 (June 1, 2015): 2015JA020983. doi:10.1002/2015JA020983.

Russell, C. T., and R. C. Elphic. "Initial ISEE Magnetometer Results: Magnetopause Observations." *Space Science Reviews* 22, no. 6 (December 1, 1978): 681–715. doi:10.1007/BF00212619.

Russell, C. T., and R. C. Elphic. "ISEE Observations of Flux Transfer Events at the Dayside Magnetopause." *Geophysical Research Letters* 6, no. 1 (January 1, 1979): 33–36. doi:10.1029/GL006i001p00033.

Russell, C. T., B. J. Anderson, W. Baumjohann, K. R. Bromund, D. Dearborn, D. Fischer, G. Le, et al. "The Magnetospheric Multiscale Magnetometers." *Space Science Reviews* 199, no. 1–4 (March 1, 2016): 189–256. doi: 10.1007/s11214-014-0057-3.

Russell, C. T., Mellott, M. M., Smith, E. J., and King, J. H.: Multiple Spacecraft Observations of Interplanetary Shocks: Four Spacecraft Determination of Shock Normals, J. Geophys. Res., 88, 4739–4748, 1983.

Yamada, 1999, Review of controlled laboratory experiments on physics of magnetic reconnection, journal of geophysical research, vol. 104, no. a7, pages 14,529–14,541.

Oka, M., T. D. Phan, S. Krucker, M. Fujimoto, and I. Shinohara, Electron Acceleration by Multi-Island Coalescence, Astrophys. J. 714, 915 (2010).

Øieroset, M., T. D. Phan, J. P. Eastwood, M. Fujimoto, W. Daughton, M. A. Shay, V. Angelopoulos, et al. "Direct Evidence for a Three-Dimensional Magnetic Flux Rope Flanked by Two Active Magnetic Reconnection X Lines at Earth's Magnetopause." *Physical Review Letters* 107, no. 16 (October 13, 2011): 165007. doi:10.1103/PhysRevLett.107.165007.

Øieroset, M., et al. (2016), MMS observations of large guide field symmetric reconnection between colliding reconnection jets at the center of a magnetic flux rope at the magnetopause, Geophys. Res. Lett., 43, 5536–5544, doi: 10.1002/2016GL069166.

Phan, T. D., et al. (2004), Cluster observations of continuous reconnection at the magnetopause under steady interplanetary magnetic field conditions, Ann. Geophys., 22, 2355–2367, doi:10.5194/angeo-22-2355-2004.

Phan, T. D., M. A. Shay, C. C. Haggerty, J. T. Gosling, J. P. Eastwood, M. Fujimoto, K. Malakit, et al. "Ion Larmor Radius Effects near a Reconnection X Line at the Magnetopause: THEMIS Observations and Simulation Comparison." *Geophysical Research Letters* 43 (September 1, 2016): 8844–52. doi:10.1002/2016GL070224.

Pollock, C., T. Moore, A. Jacques, J. Burch, U. Gliese, Y. Saito, T. Omoto, et al. "Fast Plasma Investigation for Magnetospheric Multiscale." *Space Science Reviews* 199, no. 1–4 (March 1, 2016): 331–406. doi: 10.1007/s11214-016-0245-4.

Robert, P., M. W. Dunlop, A. Roux, and G. Chanteur (1998), Accuracy of current density determination, in Analysis Methods for Multi-Spacecraft Data, edited by G. Paschmann and P. W. Daly, p. 395, ESA Publ., Noordwijk, Netherlands.

Scholer, Manfred. "Magnetic Flux Transfer at the Magnetopause Based on Single X Line Bursty Reconnection." *Geophysical Research Letters* 15, no. 4 (April 1, 1988): 291–94. doi:10.1029/GL015i004p00291.

Shay, M. A. , Drake, J. F., Rogers, B. N. and Denton, R. E., "The scaling of collisionless, magnetic reconnection for large systems ."Geophys. Res. Lett. 26, 2163 (1999).

Shue, J.-H., J. K. Chao, H. C. Fu, C. T. Russell, P. Song, K. K. Khurana, and H. J. Singer. "A New Functional Form to Study the Solar Wind Control of the Magnetopause Size and Shape." *Journal of Geophysical Research: Space Physics* 102, no. A5 (May 1, 1997): 9497–9511. doi:10.1029/97JA00196.

Silveira, M. V., W. D. Gonzalez, D. G. Sibeck, and D. Koga. "Study on Flux Transfer Events at the Earth's Magnetopause Observed by THEMIS Satellites." *AGU Fall Meeting Abstracts* 13 (December 1, 2012). http://adsabs.harvard.edu/abs/2012AGUFMSM13A2335S.

Song, H.Q., Y. Chen, G. Li, and X. L. Kong (2012), Coalescence of macroscopic magnetic islands and electron acceleration from STEREO observation, Phys. Rev. X, 2, 021015.

Sönnerup, B. U. Ö ., and M. Scheible (1998), Minimum and maximum variance analysis, in Analysis Methods for Multi-Spacecraft Data, edited by G. Paschmann and P. W. Daly, pp. 185 – 220, Int. Space Sci. Inst., Bern.

Sönnerup, B. U. Ö., H. Hasegawa, and G. Paschmann. "Anatomy of a Flux Transfer Event Seen by Cluster." *Geophysical Research Letters* 31, no. 11 (June 1, 2004): L11803. doi:10.1029/2004GL020134.

Southwood, D. J., C. J. Farrugia, and M. A. Saunders. "What Are Flux Transfer Events?" *Planetary and Space Science* 36, no. 5 (May 1, 1988): 503–8. doi:10.1016/0032-0633(88)90109-2.

Stenzel, R. L., and W. Gekelman. "Experiments on Magnetic-Field-Line Reconnection." *Physical Review Letters* 42, no. 16 (April 16, 1979): 1055–57. doi:10.1103/PhysRevLett.42.1055.

Teh, W.-L., et al. (2010), THEMIS observations of a secondary magnetic island within the Hall electromagnetic field region at the magnetopause, Geophys. Res. Lett., 37, L21102, doi: 10.1029/2010GL045056.

Torbert, R. B., C. T. Russell, W. Magnes, R. E. Ergun, P.-A. Lindqvist, O. LeContel, H. Vaith, et al. "The FIELDS Instrument Suite on MMS: Scientific Objectives, Measurements, and Data Products." *Space Science Reviews* 199, no. 1–4 (March 1, 2016): 105–35. doi:10.1007/s11214-014-0109-8.

Trenchi, L., R. C. Fear, K. J. Trattner, B. Mihaljcic, and A. N. Fazakerley. "A Sequence of Flux Transfer Events Potentially Generated by Different Generation Mechanisms." *Journal of Geophysical Research (Space Physics)* 121 (September 1, 2016): 8624–39. https://doi.org/10.1002/2016JA022847.

Walsh, B. M., T. D. Phan, D. G. Sibeck, and V. M. Souza. "The Plasmaspheric Plume and Magnetopause Reconnection." *Geophysical Research Letters* 41, no. 2 (January 28, 2014): 223–28. doi:10.1002/2013GL058802.

Wild, J. A., Cowley, S. W. H., Davies, J. A., Khan, H., Lester, M., Milan, S. E., Provan, G., Yeoman, T. K., Balogh, A., Dunlop, M. W., Fornacon, K.-H., and Georgescu, E.: First simultaneous observations of flux transfer events at the high-latitude magnetopause by the Cluster spacecraft and pulsed radar signatures in the conjugate ionosphere by the CUTLASS and EISCAT radars, Ann. Geophys., 19, 1491–1508, 2001.

Young, D. T., J. L. Burch, R. G. Gomez, A. De Los Santos, G. P. Miller, P. Wilson, N. Paschalidis, et al. "Hot Plasma Composition Analyzer for the Magnetospheric Multiscale Mission." *Space Science Reviews* 199, no. 1–4 (March 1, 2016): 407–70. doi:10.1007/s11214-014-0119-6.

Zhong, J., et al. (2013), Three-dimensional magnetic flux rope structure formed by multiple sequential X-line reconnection at the magnetopause, *J. Geophys. Res. Space Physics*, 118, 1904–1911, doi:10.1002/jgra.50281.Zhou, M., Y. Pang, X. Deng, S. Huang, and X. Lai (2014), Plasma physics of magnetic island coalescence during magnetic reconnection, J. Geophys. Res. Space Physics, 119, 6177–6189, doi: 10.1002/2013JA019483.

.

Figure 1. Solar wind conditions from the OMNI 1 minute resolution database from 06 November 2015-00:00 UT through 09 November 2015-12:00 UT. (a) Interplanetary magnetic field components in GSE coordinates, (b) Disturbance Storm Time index. Solar wind conditions during 08:00-20:00 UT on 7 November 2015, (c) Interplanetary magnetic field components in GSE coordinates, (d) solar wind dynamic ram pressure, and (e) Alfvén Mach number.

Figure 2. MMS orbit on November 7, 2015 and the normal to the magnetopause (green arrow) corresponding to the spacecraft location in the ecliptic plane. The red line corresponds to the crossing of a boundary layer.

Figure 3. Magnetic field (panel a) from FGM, electron and ion densities (b), ion velocity (c), and electron and ion spectrograms (d, e) provided by FPI, as well as He^{2+} (f) and O^{+} (g) spectrograms from HPCA from MMS1.

Figure 4. An overview of MMS1 observations between 14:15:45 and 14:17:20 UT in GSE coordinates on 7 November 2015. (a) Magnetic field components and total field strength, (b) pressures (red= plasma (ion),green= magnetic, and black= total), (c) current density from curlometer technique, (d) ion velocity components, (e) electron (black) and ion (red) densities. The black vertical dashed lines labelled T_0 to T_5, correspond to times 14:16:04; 14:16:25; 14:16:40; 14:16:43; 14:16:58 and 14:17:04.5 UT.

Figure 5. MMS1 data between 14:15:45 and 14:17:20 UT of (a) B_y and the magnetic field strength in GSE coordinates, (b) electron energy spectrum. Electron pitch angle distribution in the range of (c) 98-127 eV, (d) 451-751 eV, and (e) 3304-11551 eV.

Figure 6. (a) Magnetic field magnitude, (b)-(d) magnetic field components in the magnetopause LMN frame, (e) angle Ψ between the magnetopause normal and the magnetic field, (f)-(h) ion velocity components in the magnetopause LMN frame, (i) parallel (black) and perpendicular (red) ion velocity in the GSE coordinates system. The black vertical dashed lines labelled T_0 to T_5 are shown at the same times as in Figure 4.

Figure 7. B_y component of the magnetic field in the GSE coordinates system from the four MMS spacecraft. The horizontal dashed lines represents the several contours of different B_y values that were used to calculate their normal directions and propagation velocities.

Figure 8. The relative orientations of the PCS frame vectors $\vec{U}_P$, $\vec{U}_J$ and $\vec{U}_V$ and the GSE axes. The thick violet arrow shows the direction of the current sheet propagation velocity obtained from multi-spacecraft data analysis. The PCS frame corresponds to a translation of the GSE frame in the direction of the current sheet propagation velocity combined with a rotation about the y-GSE direction.

Figure 9. Data from MMS_1 between 14:16:38 and 14:16:44 UT (a) current density components in the GSE coordinates system, (b) parallel, perpendicular and the total current densities, (c) electrons and ions current densities as well as the current density obtained from the curlometers technique and the current density obtained from $ne(V_i - V_e)$, (d) current density components in the PCS frame, (e) magnetic field components in the PCS frame, (f) ion velocity components in the PCS frame, (g) ion velocity components in the PCS frame between 14:16:05 and 14:17:20 UT.

Figure 10. A schematic view of the crossing of the current structure in the PCS frame. The orange, green and magenta arrows show the magnetic field orientation in the FT_A, current structure and FT_B respectively. The black arrows in the $\vec{U}_J$ ($\vec{U}_V$) direction correspond to the main (bipolar) current density. The two oppositely directed red arrows in the $\vec{U}_P$ direction illustrate the compression of the current structure. The red arrows with yellow edges show the ion jet observed in the current structure. The spacecraft trajectory across the structure is represented by the dashed black arrow.

Table 1. Local magnetopause coordinate system obtained from the minimum variance analysis of the magnetic field:

		L	M	N
MP	x_{GSE}	0.24	0.48	0.84
	y_{GSE}	0.53	-0.79	0.3
	z_{GSE}	0.81	0.37	-0.44

$\lambda_L/\lambda_M = 5.75$
$\lambda_L/\lambda_N = 18.64$
$\lambda_M/\lambda_N = 3.23$

Table 2. The normal directions and the velocities of the propagating structure obtained by performing the timing method for multiple values of B_y. Mean value are: V = 66.88 km/s and N_c= [-0.5456, -0.0308, 0.8375].

B_y (nT)	N_x	N_y	N_z	V (km/s)
33	-0.5026	0.0040	0.8645	66.08
20	-0.4621	-0.1507	0.8739	60.36
15	-0.5038	-0.2519	0.8263	74.00
5	-0.5915	-0.0201	0.8061	63.63
1	-0.6140	-0.0805	0.7852	73.65
0	-0.5969	-0.0708	0.7992	73.39
-5	-0.5822	0.0018	0.8131	81.04
-35	-0.4206	0.0120	0.9072	58.43
-40	-0.5755	0.2827	0.7674	51.33

Table 3. Results of the variance analysis of the current density obtained from the curlometer technique.

		x_1	x_2	x_3
Current principal axis	x_{GSE}	-0.76	0.03	-0.65
	y_{GSE}	-0.2	-0.96	-0.19
	z_{GSE}	-0.61	0.28	0.74

$\lambda_1/\lambda_2 = 2.8$
$\lambda_1/\lambda_3 = 43.2$
$\lambda_2/\lambda_3 = 15.43$

Table 4. The unit vectors defining the PCS (Propagating Current Structure) frame:

		U_P	U_J	U_V
PCS	x_{GSE}	-0.6124	0.7676	0.1889
	y_{GSE}	0.0239	-0.2209	0.9750
	z_{GSE}	0.7902	0.6016	0.1169

Figure 1.

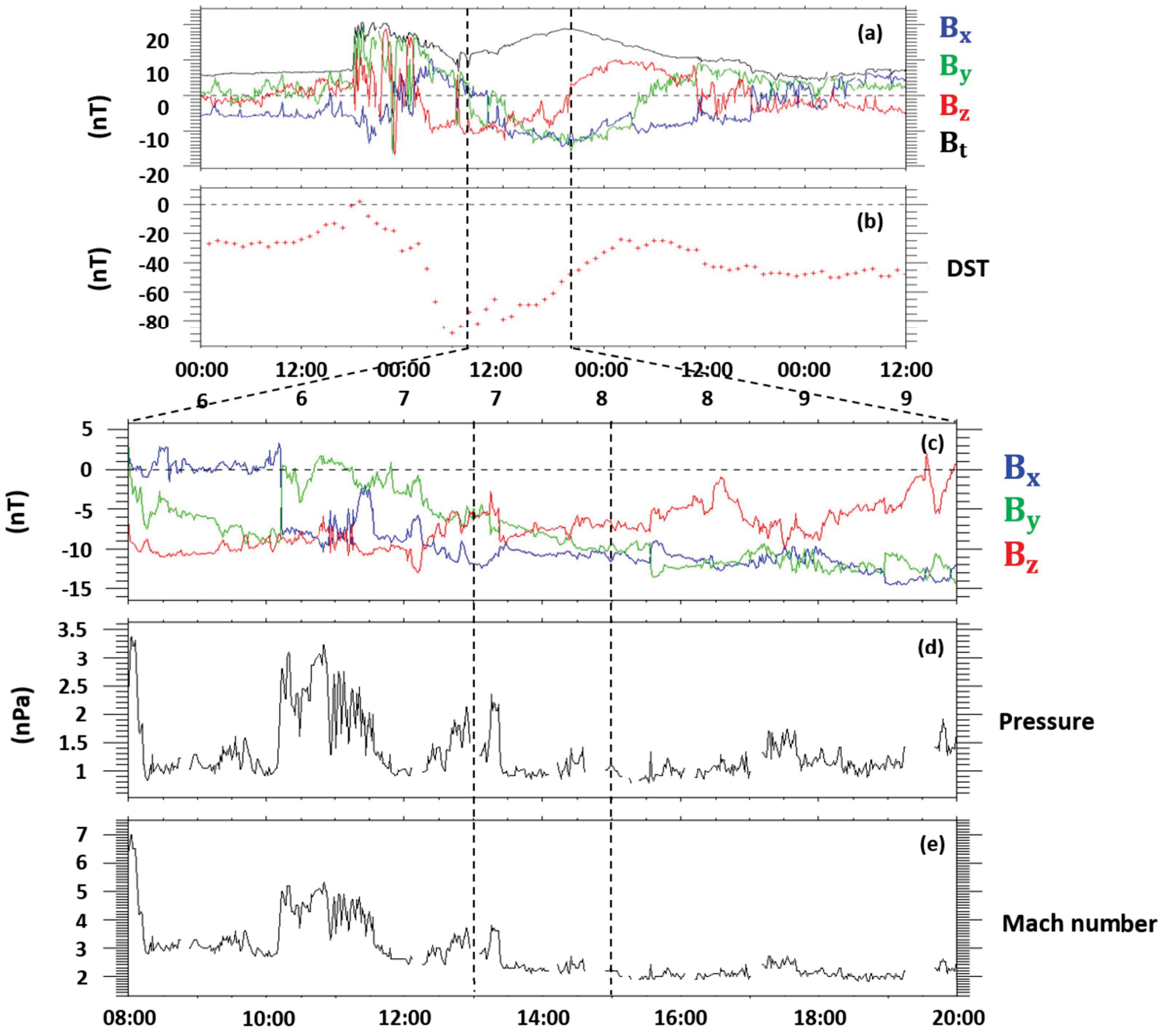
(a)
(nT)
20
10
0
-10
-20
B_x
B_y
B_z
B_t
(b)
(nT)
0
-20
-40
-60
-80
DST
00:00
12:00
00:00
12:00
00:00
12:00
00:00
12:00
6
6
7
7
8
8
9
9
(c)
(nT)
5
0
-5
-10
-15
B_x
B_y
B_z
(d)
(nPa)
3.5
3
2.5
2
1.5
1
Pressure
(e)
7
6
5
4
3
2
Mach number
08:00
10:00
12:00
14:00
16:00
18:00
20:00

Figure 2.

MMS Location for 2015-11-07 14:15:00 UTC

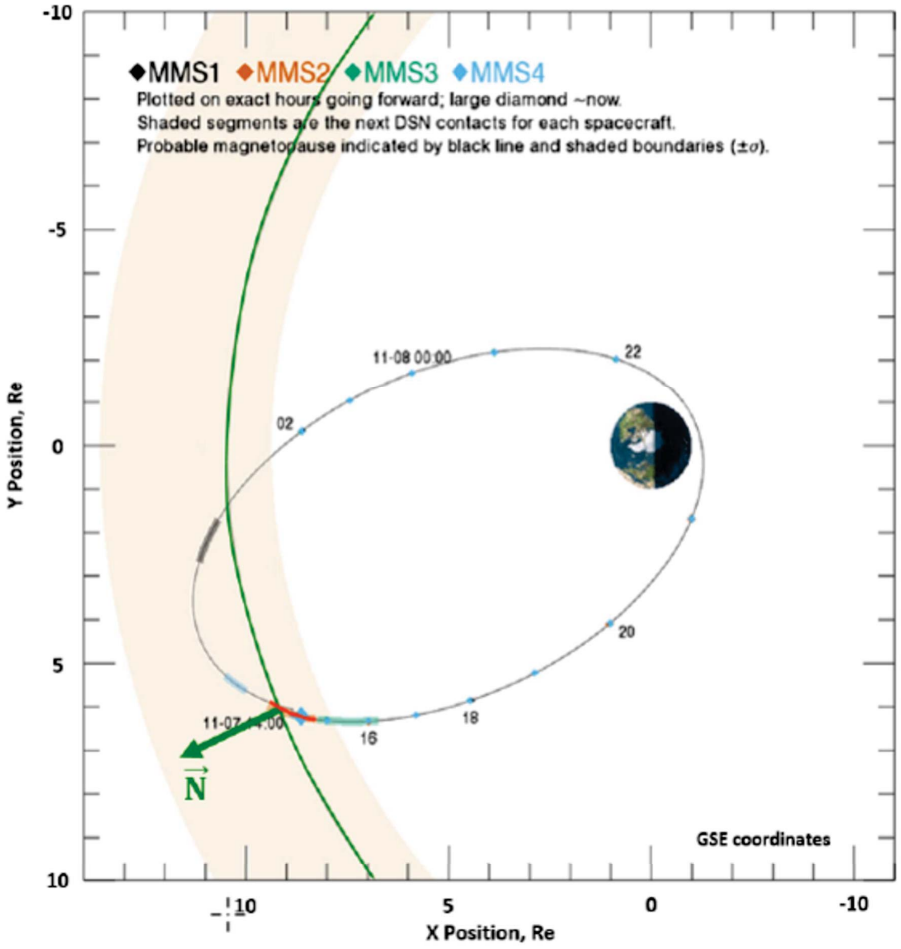

Figure 3.

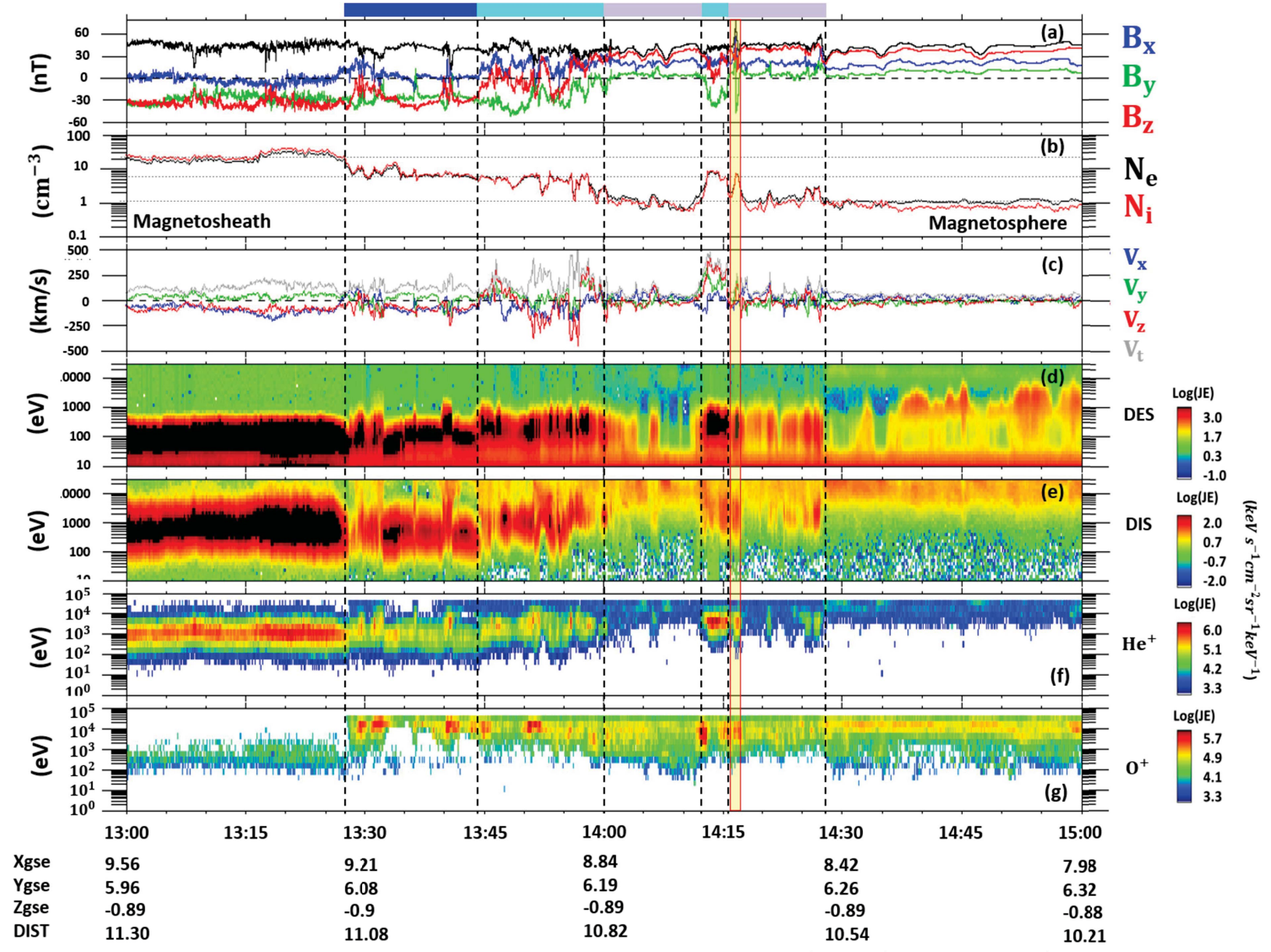

Xgse	9.56		9.21		8.84		8.42	7.98
Ygse	5.96		6.08		6.19		6.26	6.32
Zgse	-0.89		-0.9		-0.89		-0.89	-0.88
DIST	11.30		11.08		10.82		10.54	10.21

Figure 4.

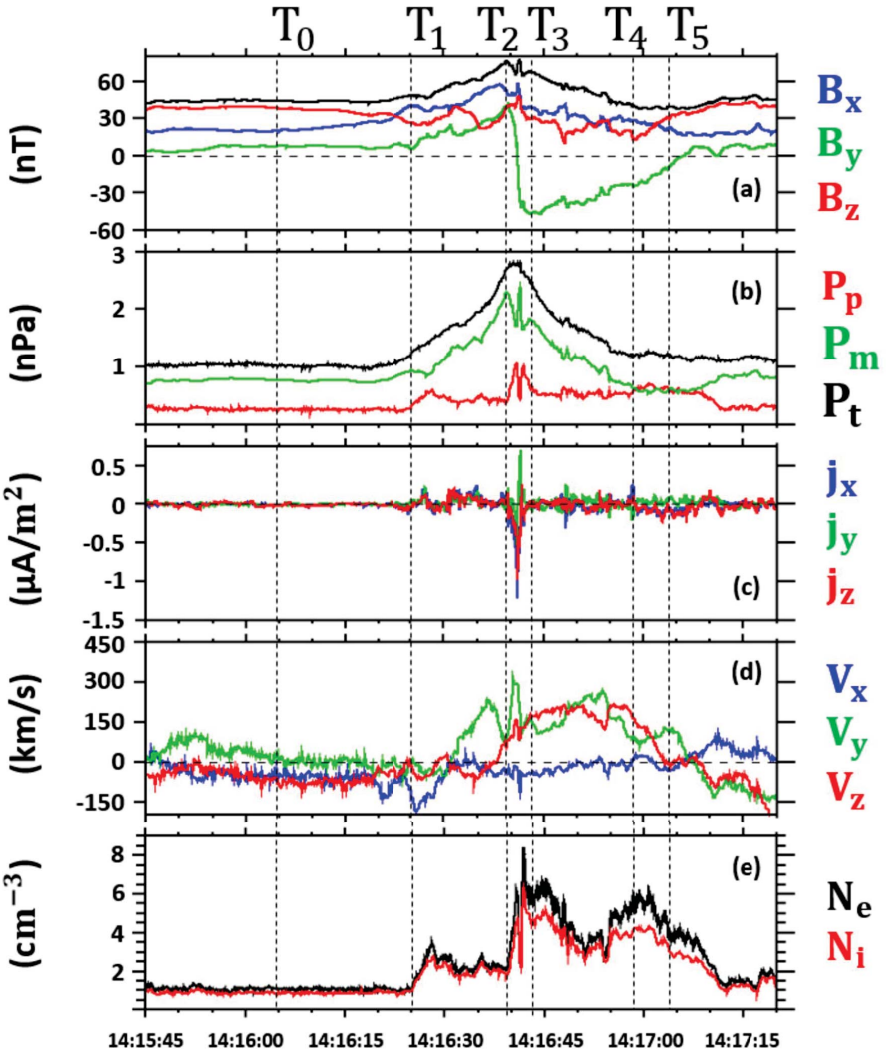
T0
T1
T2
T3
T4
T5
(nT)
60
30
0
-30
-60
(a)
Bx
By
Bz
(nPa)
3
2
1
(b)
Pp
Pm
Pt
(μA/m2)
0.5
0
-0.5
-1
-1.5
(c)
jx
jy
jz
(km/s)
450
300
150
0
-150
(d)
Vx
Vy
Vz
(cm−3)
8
6
4
2
(e)
Ne
Ni
14:15:45
14:16:00
14:16:15
14:16:30
14:16:45
14:17:00
14:17:15

Figure 5.

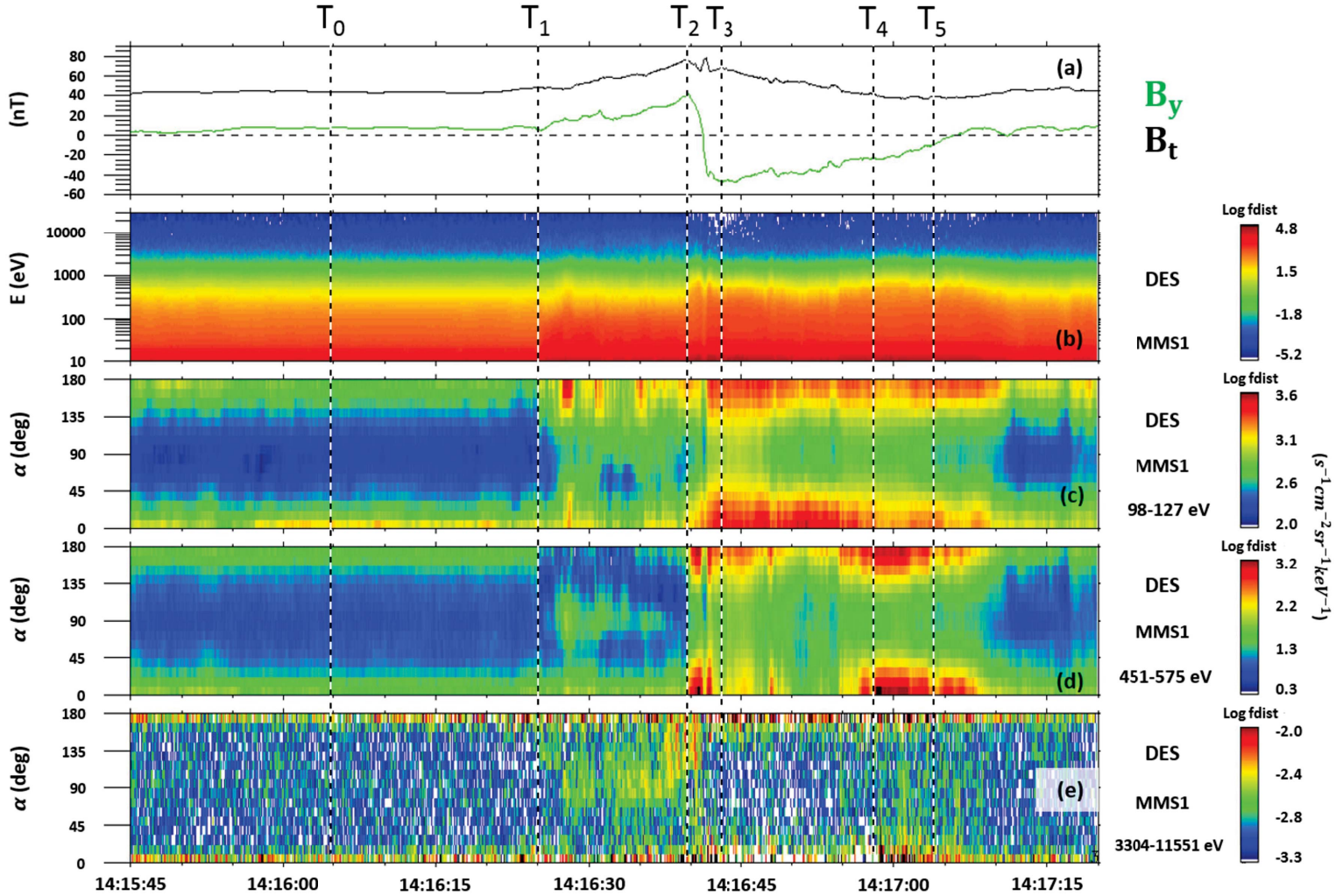
T0
T1
T2
T3
T4
T5
(nT)
80
60
40
20
0
-20
-40
-60
(a)
By
Bt
E (eV)
10000
1000
100
10
(b)
DES
MMS1
Log fdist
4.8
1.5
-1.8
-5.2
α (deg)
180
135
90
45
0
(c)
DES
MMS1
98-127 eV
Log fdist
3.6
3.1
2.6
2.0
(d)
DES
MMS1
451-575 eV
Log fdist
3.2
2.2
1.3
0.3
(e)
DES
MMS1
3304-11551 eV
Log fdist
-2.0
-2.4
-2.8
-3.3
$(s^{-1}cm^{-2}sr^{-1}keV^{-1})$
14:15:45
14:16:00
14:16:15
14:16:30
14:16:45
14:17:00
14:17:15

Figure 6.

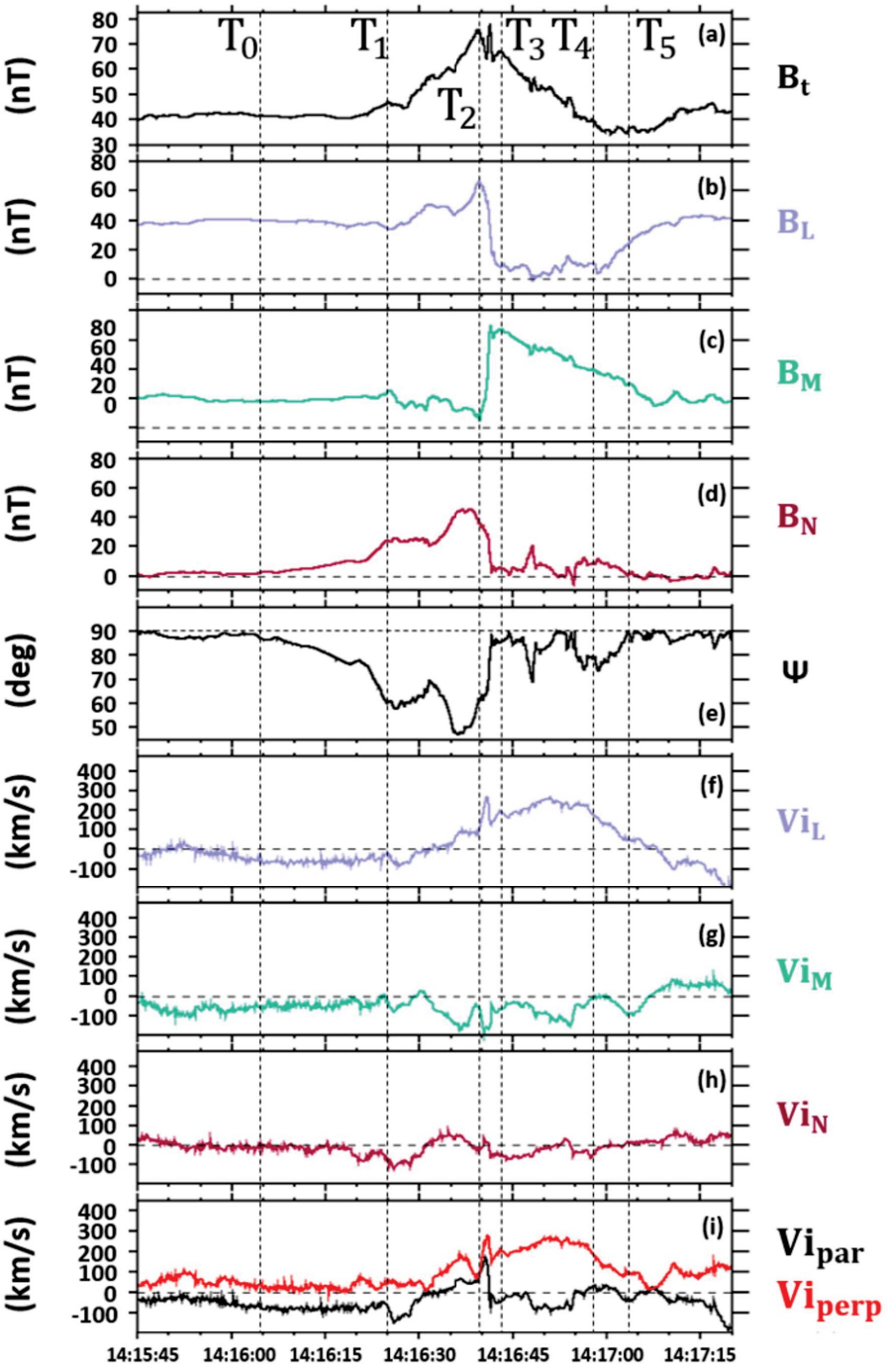
T0
T1
T2
T3
T4
T5
(a)
(b)
(c)
(d)
(e)
(f)
(g)
(h)
(i)
(nT)
(deg)
(km/s)
Bt
BL
BM
BN
ψ
ViL
ViM
ViN
Vipar
Viperp
14:15:45
14:16:00
14:16:15
14:16:30
14:16:45
14:17:00
14:17:15

Figure 7.

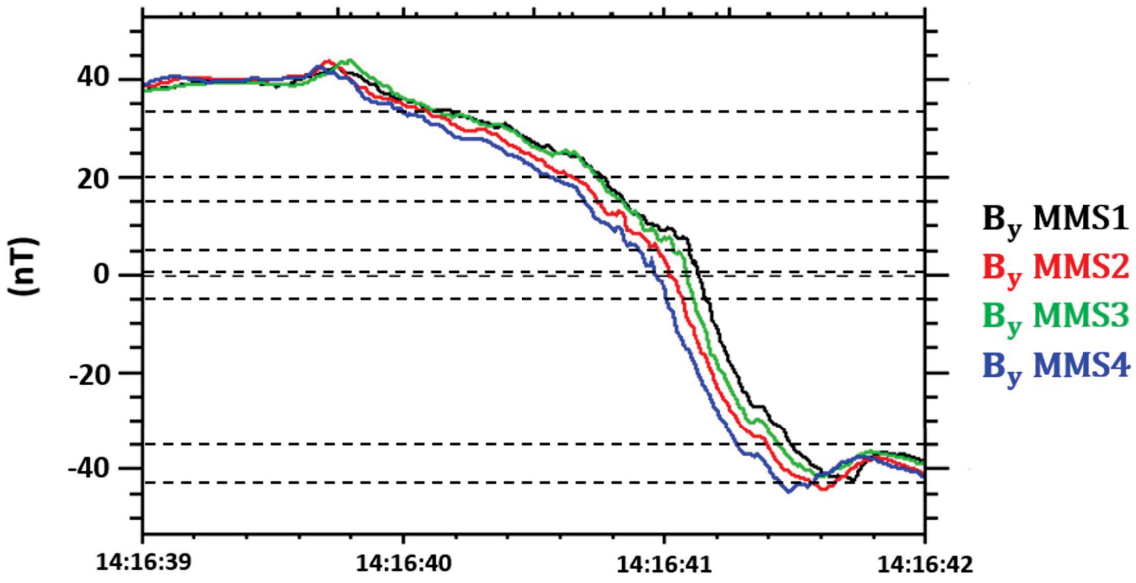
40
20
0
-20
-40
(nT)
14:16:39
14:16:40
14:16:41
14:16:42
B$_y$ MMS1
B$_y$ MMS2
B$_y$ MMS3
B$_y$ MMS4

Figure 8.

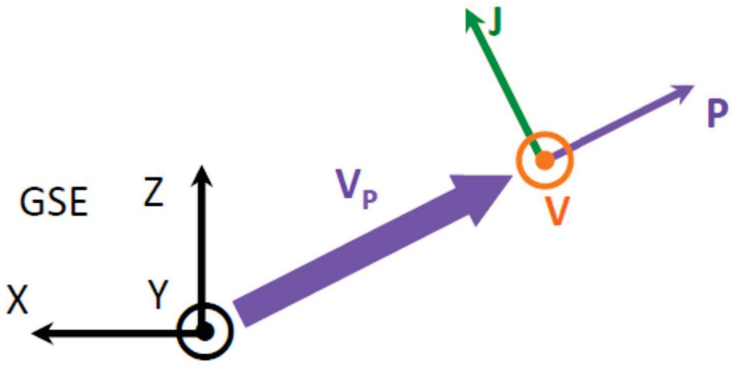
J
P
GSE
Z
V_P
V
X
Y

Figure 9.

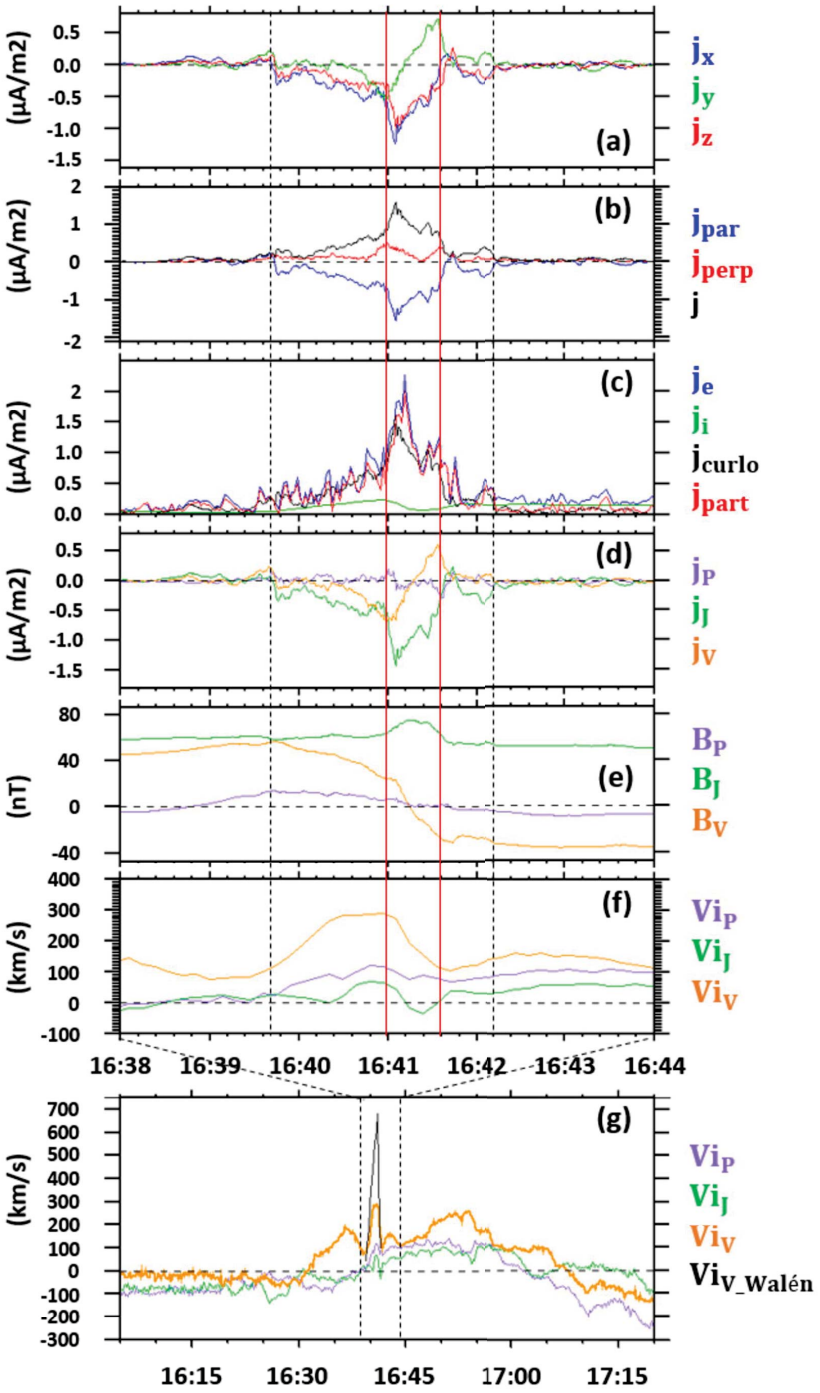
(μA/m2)
0.5
0.0
-0.5
-1.0
-1.5
(a)
jx
jy
jz
2
1
0
-1
-2
(b)
jpar
jperp
j
2
1.5
1.0
0.5
0.0
(c)
je
ji
jcurlo
jpart
(d)
jP
jJ
jV
(nT)
80
40
0
-40
(e)
BP
BJ
BV
400
300
200
100
0
-100
(km/s)
(f)
ViP
ViJ
ViV
16:38
16:39
16:40
16:41
16:42
16:43
16:44
700
600
500
400
300
200
100
0
-100
-200
-300
(g)
ViP
ViJ
ViV
ViV_Walén
16:15
16:30
16:45
17:00
17:15

Figure 10.

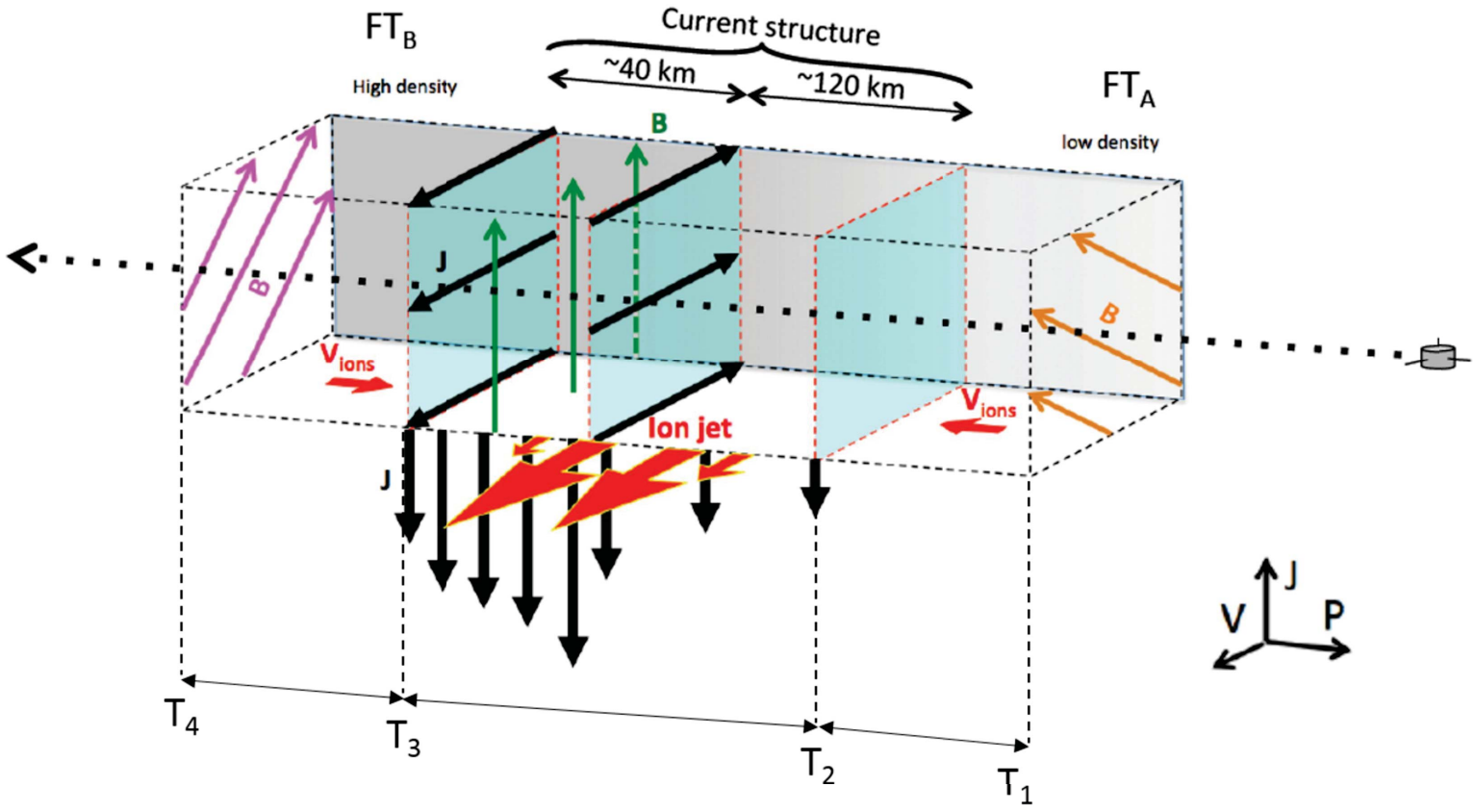
FT_B
High density
Current structure
~40 km
~120 km
FT_A
low density
B
B
J
B
V_ions
V_ions
Ion jet
J
J
V
P
T_4
T_3
T_2
T_1